Inorganic Chemistry

ARTICLE

pubs.acs.org/IC

Long-Range Spin Coupling: A Tetraphosphine-Bridged Palladium Dimer

Kuppuswamy Arumugam,[†] Mohammed C. Shaw,[†] Joel T. Mague,[†] Eckhard Bill,[‡] Stephen Sproules,*[,‡] and James P. Donahue*[,†]

[†]Department of Chemistry, Tulane University, 6400 Freret Street, New Orleans, Louisiana 70118-5698, United States

[‡]Max-Planck-Institut für Bioanorganische Chemie, Stiftstrasse 34-36, D-45470 Mülheim an der Ruhr, Germany

Supporting Information

ABSTRACT: The dipalladium compound [{(adt)Pd}$_2$(μ-tpbz)] (**1**) (adt = bis(*p*-anisyl)-1,2-ethylenedithiolate, tpbz = 1,2,4,5-tetrakis(diphenylphosphino)benzene) has been synthesized from [{Cl$_2$Pd}$_2$(μ-tpbz)] by transmetalation employing (adt)SnMe$_2$. The cyclic voltammogram (CV) of **1** reveals reversible oxidation waves at 0.00 V and +0.50 V (vs [Fc]$^+$/Fc) with current amplitude twice that for identical processes in the monopalladium compound [(adt)Pd(dppb)] (**2**) (dppb = 1,2-bis(diphenylphosphino)benzene), an observation indicating each wave involves simultaneous one-electron oxidations at each metallodithiolene fragment. This assignment is affirmed by density functional theory (DFT) calculations that show the redox-active molecular orbital (MO) is principally composed of the dithiolene S$_2$C$_2$ π-system, and by spectroelectrochemical UV−vis of [**1**]$^{2+}$, which displays hallmark low energy charge transfer (CT) bands. Dication [**1**]$^{2+}$ is a diradical with a near degenerate singlet−triplet ground state; fluid solution electron paramagnetic resonance (EPR) spectra validate the DFT-derived isotropic exchange coupling, $J' = -6.3$ cm^{-1}. The frozen solution X-band EPR spectrum of [**1**]$^{2+}$ is consistent with a spin-triplet bearing a very faint half-field ("$\Delta M_S = 2$") signal. It is successfully simulated with an amazingly small zero field splitting, $D = -15 \times 10^{-4}$ cm^{-1} and negligible rhombicity ($E/D = 0.008$). These zero-field splitting parameters, which stem from the long-range dipolar spin coupling, are very accurately reproduced using a multipoint dipole model with an optimized interspin distance of 12.434 Å. With the framework reported herein for understanding how the weak interaction of two spins is mediated by tpbz, this bridging ligand can now be incorporated into extended systems with tailored chemical and physical properties for use in a variety of molecular-based electronic and magnetic devices.

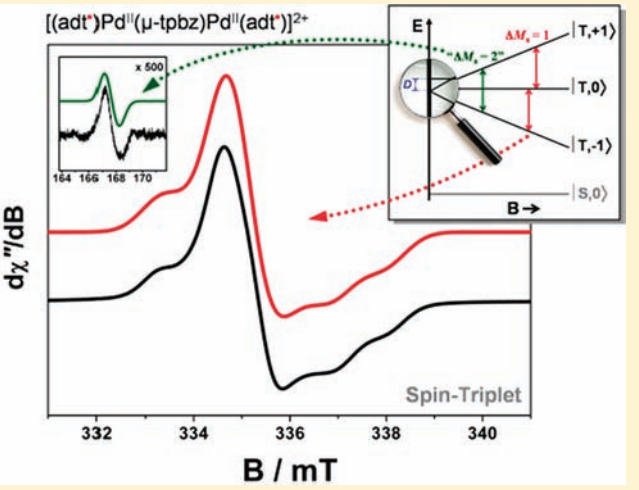

INTRODUCTION

The development of materials with specific magnetic properties is advanced by a molecule-level synthetic ability to incorporate multiple electron spins at well-defined distances and geometric arrangements such that the magnitude of the resulting spin coupling is both understandable and controllable. The potent combination of coordination chemistry and supramolecular chemistry has demonstrated this technique in abundance.[1] However, beyond topological design, control over subsequent magnetic properties is derived from understanding the intrinsic electronic structure of elementary building blocks. For instance, the rigidly planar 1,2,4,5-tetrakis(diphenylphosphino)benzene (tpbz) unit has been previously incorporated into bimetallic complexes with the expressed wish to extend to conducting organometallic polymers.[2,3] Fox and co-workers revealed such systems were feeble conductors because the intermetallic electronic coupling was greatly attenuated by localization of the metal spins by the tpbz ligand. However, the insulating effect of this bridging ligand could be exploited to investigate the long-range coupling of spins for use in devices that desire weak coupling, such as spin qubits in the development of quantum computing.[4] In this context, we have synthesized a dipalladium compound, [{(adt)Pd}$_2$(μ-tpbz)] (**1**), in which metal centers are bridged by the tpbz ligand, and the ends of the molecule are capped with redox active bis(*p*-anisyl)-1,2-ethylenedithiolate (adt)$^{2-}$ ligands (Scheme 1). This compound is related to a recently reported set of arenetetrathiolate-linked dimetal compounds with terminal chelating phosphine ligands,[5] compounds which differ from **1** by an inversion of the nature of the bridging

Received: December 13, 2010
Published: March 07, 2011

Scheme 1. Synthesis of Tetraphosphinobenzene-Linked Group 10 Dimetal Compounds with Terminal *p*-Anisyl Substituted Dithiolene Ligands

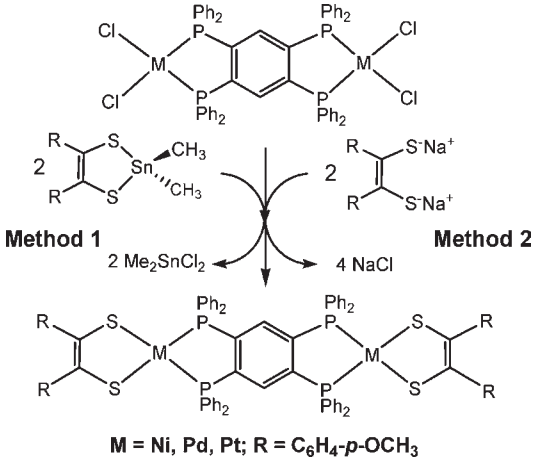

and terminal ligands. In situ electrochemical oxidation of the two end groups generates a dicationic complex $[\{(adt)Pd\}_2(\mu\text{-tpbz})]^{2+}$, with a degenerate singlet−triplet ground state. As elegantly demonstrated by Eaton and Eaton,[6−8] traditional magnetic susceptibilty measurements are transcended by continuous wave electron paramagnetic resonance (EPR) spectroscopy for the determination of exchange and dipolar interactions for paramagnetic molecules exhibiting magnetic interactions weaker than kT. The resulting analysis of $[\mathbf{1}]^{2+}$ yields an amazingly small zero-field splitting (D) parameter for this spin-triplet with negligible rhombicity (E/D).

EXPERIMENTAL SECTION

All syntheses were carried out under a dinitrogen atmosphere using standard Schlenk techniques. The ligands 1,2,4,5-tetrakis(diphenylphosphino)benzene[9] (tpbz) and 1,2-bis(diphenylphosphino)benzene[10] (dppb) and the palladium compounds $[\{Cl_2Pd\}_2(\mu\text{-tpbz})]$[11] and $[Cl_2Pd(dppb)]$[9a] were prepared by literature routes. The protected dithiolene ligand, 4,5-bis(4-methoxyphenyl)-2,2-dimethyl-1,3,2-dithiastannole, $[(adt)Sn(Me)_2]$, was prepared by analogy to a related compound.[12] Solvents either were dried with a system of drying columns from the Glass Contour Company (CH_2Cl_2, Et_2O) or were freshly distilled according to standard procedures (1,2-dichloroethane, MeOH).[13]

$[\{(adt)Pd\}_2(\mu\text{-tpbz})]$, 1. A 25 mL Schlenk flask was charged with $[\{Cl_2Pd\}_2(\mu\text{-tpbz})]$ (0.140 g, 0.12 mmol) and 4,5-bis(4-methoxyphenyl)-2,2-dimethyl-1,3,2-dithiastannole, $[(adt)Sn(Me)_2]$, (0.100 g, 0.22 mmol) in dry CH_2Cl_2 (15 mL). The resulting heterogeneous mixture was stirred for 12 h at 25 °C under N_2, during which time the insoluble $[\{Cl_2Pd\}_2(\mu\text{-tpbz})]$ completely dissolved, and a homogeneous dark brown solution formed. This solution was taken to dryness under reduced pressure. The resulting brown solid residue was washed with MeOH (3 × 5 mL) followed by Et_2O (3 × 5 mL) and was then dried under vacuum. Yield: 0.140 g (72%). ^{1}H NMR (δ, ppm in CD_2Cl_2): 7.59−7.63 (m, 2H, aromatic C-*H*), 7.43−7.48 (m, 24H, aromatic C-*H*), 7.31−7.35 (m, 16H, aromatic C-*H*), 7.03 (d, 8H, J = 8.6 Hz, aromatic C-*H*), 6.59 (d, 8H, J = 8.8 Hz, aromatic C-*H*), 3.68 (s, 12H, dithiolene $-OCH_3$). ^{13}C NMR (δ, ppm in CH_2Cl_2): 55.0, 112.7, 128.9, 129.3, 131.0, 133.4, 136.3, 149.9, 157.7. ^{31}P NMR (δ, ppm in CD_2Cl_2): 47.11. UV/vis (CH_2Cl_2): λ_{max} (ε) = 492 nm (3100) M^{-1} cm^{-1}. MS (MALDI-TOF): 1632.3 (M^+). HRMS (MALDI-TOF): monoisotopic m/z: 1632.2838 (calcd for $C_{86}H_{70}O_4P_4Pd_2S_4$ (M^+) 1632.1181). Anal. Calcd for $[\{(adt)Pd\}_2(\mu\text{-tpbz})]$, $C_{86}H_{70}O_4P_4Pd_2S_4$: C, 63.27; H, 4.32; P, 7.59; Found: C, 62.39; H, 4.26; P, 7.95.

Table 1. Crystallographic Data for 1 and $2\cdot2(ClCH_2CH_2Cl)$

	1	$2\cdot2(ClCH_2CH_2Cl)$
formula	$C_{86}H_{70}O_4P_4Pd_2S_4$	$C_{50}H_{46}Cl_4O_2P_2PdS_2$
fw	1632.34	1053.13
space group	$P\bar{1}$	$P\bar{1}$
a, Å	20.988(4)	11.8736(9)
b, Å	28.799(5)	13.304(1)
c, Å	31.661(7)	16.235(1)
α, deg.	80.994(4)	96.101(1)
β, deg.	76.492(2)	90.613(1)
γ, deg.	76.029(3)	112.865(1)
V, Å^3	17955(6)	2345.8(3)
Z	8	2
T, K	100(2)	100(2)
ρ calcd, g·cm^{-3}	1.208	1.491
refl. collected/$2\Theta_{max}$	147328	41028
unique refl./$I > 2\sigma(I)$	69710	11240
No. of params/restr.	2841/58	552/0
λ, Å/μ(Kα), mm^{-1}	0.71073/0.608	0.71073/0.821
R1[a]/goodness of fit[b]	0.0780/1.180	0.0280/1.031
wR2[c] ($I > 2\sigma(I)$)	0.1627	0.0641
residual density, e·Å^{-3}	1.498, −1.279	0.781, −0.683

[a] Observation criterion: $I > 2\sigma(I)$. R1 = $\sum||F_o| - |F_c||/\sum|F_o|$. [b] GoF = $[\sum w(F_o^2 - F_c^2)^2]/(n-p)]^{1/2}$. [c] wR2 = $[\sum[w(F_o^2 - F_c^2)^2]/\sum[w(F_o^2)^2]]^{1/2}$ where $w = 1/[\sigma^2(F_o^2) + (aP)^2 + bP]$, $P = [2F_c^2 + \mathrm{Max}(F_o^2,0)]/3$.

[(adt)Pd(dppb)], 2. A 50 mL Schlenk flask was charged with 4,5-bis(4-methoxyphenyl)-2,2-dimethyl-1,3,2-dithiastannole, $[(adt)Sn(Me)_2]$, (0.100 g, 0.22 mmol) and $[Cl_2Pd(dppb)]$ (0.138 g, 0.22 mmol). To this mixture of solids was added 25 mL of CH_2Cl_2, which occasioned an immediate change in color from orange to dark brown. This solution was stirred overnight at ambient temperature and then was evaporated to dryness under reduced pressure. The residual solid was washed with MeOH (3 × 10 mL) and Et_2O (3 × 10 mL) and dried again in vacuo to afford a brown solid. Yield: 0.104 g (55%). Recrystallization was readily accomplished by the diffusion of *n*-pentane vapor into a filtered CH_2Cl_2 or $ClCH_2CH_2Cl$ solution. ^{1}H NMR (CD_2Cl_2): δ 7.68−7.58 (m, 12H, aromatic C-*H*), 7.48−7.45 (m, 4H, aromatic C-*H*), 7.41−7.36 (m, 8H, aromatic C-*H*), 7.06 (d, 4H, aromatic C-*H* of adt ligand), 6.60 (d, 4H, aromatic C-*H* of adt ligand), 3.69 (s, 6H, -OCH_3). ^{31}P NMR (CD_2Cl_2): 50.08 (s). UV/vis (CH_2Cl_2): λ_{max} (ε) = 541 (500), 541 nm (1400) M^{-1} cm^{-1}. MS (MALDI-TOF): 855.1 (M^+). HRMS (MALDI-TOF): monoisotopic m/z: 854.0823 (calcd for $C_{46}H_{38}O_2P_2PdS_2$ (M^+) 854.0832). Anal. Calcd for $[(adt)Pd(dppb)]\cdot11/2CH_2Cl_2$, $C_{47.5}H_{41}Cl_3O_2P_2PdS_2$: C, 58.06; H, 4.21; P, 6.30; Found: C, 57.82; H, 4.27; P, 6.53.

Crystallography. Orange block-shaped crystals of **1** grew by diffusion of 1,2-dimethoxyethane vapor into a chlorobenzene solution, while red plates of $\mathbf{2}\cdot2ClCH_2CH_2Cl$ were similarly obtained by slow introduction of hexanes vapor into a 1,2-dichloroethane solution (Table 1). Data were collected with a Bruker APEX CCD diffractometer equipped with a Kryoflex attachment supplying a nitrogen stream at 100 K. Data were collected under control of the APEX2 program suite.[14] For **1**, a full sphere of data was obtained by collecting three sets of 606 frames (0.3 deg. width in ω) at φ = 0, 120, and 240 degrees with a scan time of 70 s/frame. From 3699 reflections chosen from the full data set and

having $I//s(I) > 15$, it was determined with the use of CELL_NOW[15] that the crystal was twinned by a 180° rotation about the c axis of the derived triclinic cell. The raw data were integrated using the multi-component version of SAINT under control of the two-component instruction file generated by CELL_NOW. For **2**, the diffraction data were collected in 3 sets of 400 frames, each of width 0.5 deg. in ω, collected at φ = 0.00, 90.00, and 180.00 deg and 2 sets of 800 frames, each of width 0.45 deg in φ, collected at $\omega = -30.00$ and 210.00 deg. A scan time of 15 s/frame was employed.

The raw data were reduced to F^2 values using the SAINT software,[16] and a global refinement of unit cell parameters was performed using selected reflections (9965 for **1**, 9604 for **2**) from the full data set. Multiple measurements of symmetry equivalent reflections provided the basis for an empirical absorption correction as well as a correction for any crystal decomposition during the course of the data collection (SADABS[17a] for **2**; TWINABS[17b] for **1**). Structure solutions were obtained by the Patterson method. Refinements were accomplished by full-matrix least-squares procedures using the SHELXTL software suite.[18] After considerable effort, it was concluded that the best model for **1** was one in which the single-component data set which was extracted from the full data set by TWINABS was used for refinement. For the multiple molecules in the asymmetric unit of **1**, some phenyl groups on the 1,2,4,5-tetrakis-(diphenylphosphino)benzene ligand displayed positional disorder; this disorder was generally treated with a split atom model. In many instances, distance and angle constraints were imposed by use of the AFIX 66 command. Some disorder in the *p*-CH_3O- group of the adt(2-) ligands was also observed and similarly treated with a split atom model. All hydrogen atoms were added in calculated positions and included as riding contributions with isotropic displacement parameters tied to those of the carbon atoms to which they were attached. For **1**, electron density associated with several sites partially occupied by disordered molecules of solvent chlorobenzene and 1,2-dimethoxyethane were removed with the SQUEEZE option of the PLATON package.[19] Selected crystal and refinement data for **1** and **2**·2($ClCH_2CH_2Cl$) are presented in Table 1.

Other Physical Measurements. All NMR spectra were recorded at 25 °C either with a Varian Unity Inova spectrometer operating at 400, 100.5, and 161.8 MHz for ^1H, ^{13}C, and ^{31}P, respectively, or with a Bruker AVANCE 300 spectrometer operating at 121.5 MHz for ^{31}P. Spectra were referenced to the solvent residual for ^1H and ^{13}C and to external 85% H_3PO_4 for ^{31}P. Mass spectra (MALDI-TOF) were obtained with either an ABI Voyager-DE STR instrument or a Bruker Autoflex III instrument. Electrochemical measurements were made with a CHI620C electroanalyzer workstation using a Ag/AgCl reference electrode, platinum disk working electrode, Pt wire auxiliary electrode, and [^{n}Bu$_4$N][PF_6] as the supporting electrolyte. Potentials are referenced versus the $[Fc]^+$/Fc couple, which occurred at +0.54 mV (by CV) in 0.1 M [^{n}Bu$_4$N][PF_6] in CH_2Cl_2. Electronic absorption spectra of complexes from the spectroelectrochemical measurements were recorded on a HP 8452A diode array spectrophotometer (200−1100 nm) at −25 °C. X-band EPR spectra were recorded on a Bruker ELEXSYS E500 spectrometer. The S-band EPR spectrum was measured on a Bruker ESP 300 spectrometer. Spectra were recorded in 0.1 *M* [Bu_4N][PF_6] in CH_2Cl_2. To ensure against poor glassing effects, the low temperature spectra were recorded both with the sample tube in multiple orientations and after repeated warmings and refreezings of the sample. The same spectra were consistently observed. Simulations were performed with XSophe[20] distributed by Bruker Biospin GmbH. Elemental analyses were performed by Midwest Microlab, LLC of Indianapolis, IN.

Calculations. All density functional theory (DFT) calculations were performed with the ORCA program.[21] The complexes were geometry optimized using the BP86 functional.[22] The all-electron basis sets were those reported by the Ahlrichs group.[23] Triple-ξ-quality basis sets with one set of polarization functions (def2-TZVP) were used for the palladium and the sulfur atoms. A scalar relativistic correction was applied using the zeroth-order regular approximation (ZORA) method.[24,25] In the context of ZORA, a one center approximation has been shown to introduce only minor errors to the final geometries.[24] The remaining atoms were described by slightly smaller polarized split-valence def2-SV(P) basis sets that are double-ξ-quality in the valence region and contain a polarizing set of d functions on the nonhydrogen atoms.[23] Auxiliary basis sets used to expand the electron density in the calculations were chosen to match the orbital basis. Since the compounds studied are mostly cations, we carried out the calculations in a dielectric continuum using the conductor-like screening model (COSMO).[26] The self-consistent field calculations were tightly converged (1×10^{-8} E_h in energy, 1×10^{-7} E_h in the density charge, and 1×10^{-7} in the maximum element of the DIIS[27] error vector). The geometry search for all complexes was carried out in redundant internal coordinates without imposing geometry constraints. Electronic energies and properties were calculated at the optimized geometries using the B3LYP functional.[28] In this case the same basis sets were used. We used the broken symmetry (BS) approach to describe our computational results for the dicationic compound $[\mathbf{1}]^{2+}$.[29] Canonical orbitals and density plots were obtained using Molekel.[30]

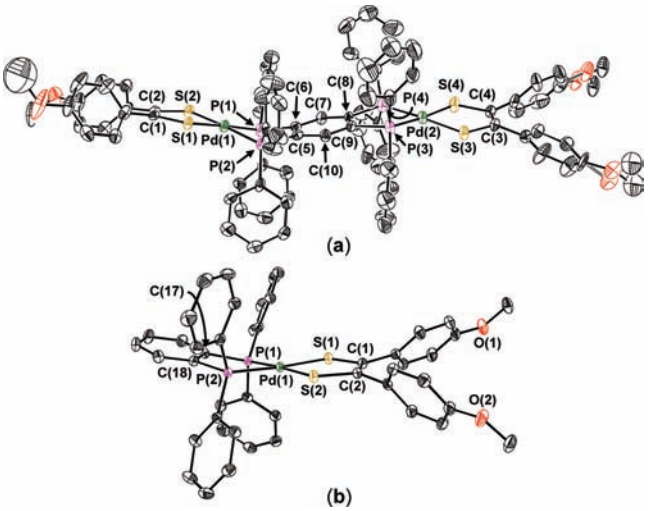

Figure 1. Thermal ellipsoid plots of (a) **1**, and (b) **2** drawn at 50% probability. H atoms are omitted for clarity.

RESULTS AND DISCUSSION

Synthesis and Structural Characterization. Compound **1** and its Ni and Pt analogues were readily prepared in yields of 60−70% from the corresponding dimetal tetrachloro compounds by trans-metalation reactions with dialkyltin-protected forms of the dithiolene ligands (Method 1, Scheme 1). We observe this approach to be generally cleaner and higher yielding than an alternative route proceeding by halide displacement from [{X_2M}$_2$(μ-tpbz)] (X = halide) with fully reduced ene-1,2-dithiolate salts (Method 2, Scheme 1). The related monopalladium dithiolene bis(phosphine) compound with the 1,2-bis(diphenylphosphino)benzene ligand (dppb), [(adt)Pd(dppb)] (**2**), has been synthesized by a similar transmetalation procedure to assist an understanding of the properties of the dimetallic molecules.

Compound **1** crystallized with an unusual asymmetric unit in $P\bar{1}$ consisting of three independent molecules and two half-molecules; one of the independent whole molecules is displayed in Figure 1 a. The tetrahedralization at each metal atom, which may be quantified by the dihedral angle between the S_2Pd and P_2Pd planes, ranges from 3.2° to 15.7° with an average of 9.0°.

dx.doi.org/10.1021/ic102493g |*Inorg. Chem.* 2011, 50, 2995–3002

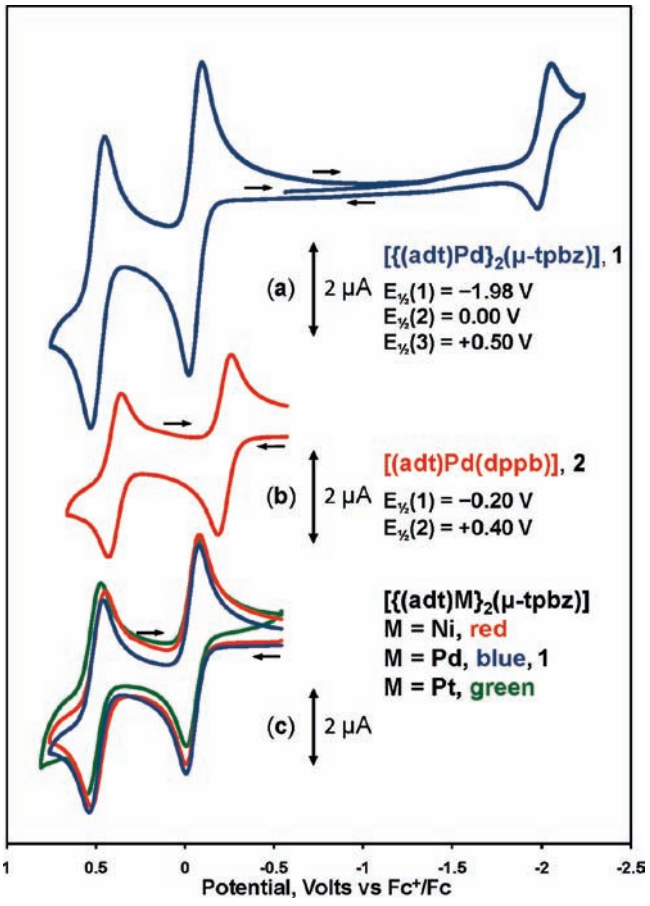

Figure 2. Cyclic voltammograms of **1** (a), **2** (b), and [{(adt)M}$_2$(μ-tpbz)] (M = Ni, Pd, Pt) (c) in CH_2Cl_2 solution (containing 0.1 *M* [^{n}Bu$_4$N][PF$_6$]) at 25 °C and a scan rate of 100 mV s^{-1}.

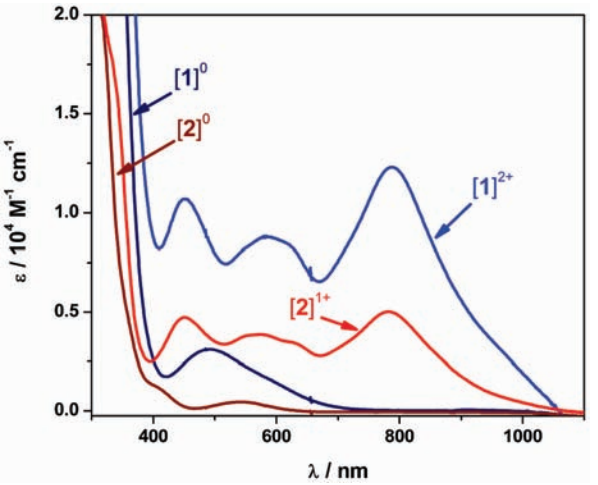

Figure 3. Electronic absorption spectra of [**1**]$^{0/2+}$ and [**2**]$^{0/1+}$ in CH_2Cl_2 solution (containing 0.1 M [^{n}Bu$_4$N][PF$_6$]) at −25 °C.

Scheme 2. Electron Transfer Series for 1

$$[(adt)Pd^{II}(\mu\text{-tpbz})Pd^{II}(adt)]^0$$
$$\overset{+2e^-}{\underset{-2e^-}{\rightleftharpoons}}$$
$$[(adt^{\bullet})Pd^{II}(\mu\text{-tpbz})Pd^{II}(adt^{\bullet})]^{2+}$$
$$\overset{+2e^-}{\underset{-2e^-}{\rightleftharpoons}}$$
$$[(adt^0)Pd^{II}(\mu\text{-tpbz})Pd^{II}(adt^0)]^{4+}$$

Angles between the S_2PdP_2 and the $P_2C_6P_2$ mean planes, which express the magnitude of the chair-type conformation visible to the molecule in Figure 1 a, range from 13.4° to 31.0°. These deviations from idealized D_{2h} point group symmetry contrast with the structure observed for [(dcpe)Pd($S_2C_6H_2S_2$)Pd(dcpe)] (dcpe = 1,2-bis(dicyclohexylphosphino)ethane),[5] which crystallized with near perfectly planar $P_2Pd(S_2C_6S_2)PdP_2$ core. Compound **2** was also characterized structurally (Figure 1 b) but was observed to have the square planar coordination geometry that is more typical for Pd(II) in this strong ligand field environment. Average C−S and C−C bond lengths for **1** are 1.771[1] and 1.348[3] Å, respectively, values consistent with fully reduced $(adt)^{2-}$ ligand bound to a Pd(II) central ion.

Spectro- and Electrochemistry. The cyclic voltammogram (CV) of **1** is shown in Figure 2 a, where two reversible oxidation waves and one reversible reduction wave are exhibited. By comparison with the CV of **2** (Figure 2 b), it is abundantly evident from the observed current amplitude that the oxidations of **1** involve concurrent one-electron processes, two-electrons in total for each oxidation wave; its reduction is a single one-electron process. This interpretation is furthered by spectroelectrochemical measurements. By controlled-potential coulometry the first oxidation wave of **1** is fully reversible, while the second set of simultaneous one-electron oxidations and the reduction process are not reversible on the time scale of the experiment. The electronic absorption spectrum of [**1**]$^{2+}$ displays an envelope of intense ($\varepsilon \approx 1.23 \times 10^4$ M^{-1} cm^{-1}) charge transfer bands in the near-IR region (>700 nm) that are absent in the spectrum of **1** (Figure 3). Similarly, [**2**]$^{1+}$ displays the same spectral profile, though the intensity of the bands in the near-IR region is about half that seen for [**1**]$^{2+}$, underscoring the notion that the tpbz ligand effectively insulates the two [Pd(dithiolene)] moieties. The presence of such intense low-energy bands, together with the complete invariance of the voltammetry when the Ni and Pt analogues of **1** (and **2**[31]) are measured (Figure 2 c), circumstantiates these oxidation events as being ligand-centered. Therefore, we have defined the three-membered electron transfer series for **1** as shown in Scheme 2.

DFT Calculations. The electronic structures of the three-membered electron transfer series for **1** and **2** in which the Ph groups of tpbz and the methoxy substituents of the dithiolene ligands have been replaced with H atoms have been determined by theoretical calculations. The geometry-optimized structures for **1** and **2** performed at the ZORA/B3LYP level closely match the experimental parameters with long C−S (1.776 Å) and short C−C (1.375 Å) interatomic distances, consistent with a dianionic ene-1,2-dithiolate(2−) form of the ligand. A slight distortion away from square planarity (α = 4.7°) was noted for each Pd center. In contrast to the crystal structure of **1**, which showed a distinct chair conformation to the Pd-tpbz-Pd unit, giving a Pd···Pd distance of 8.5 Å, the optimized structure is perfectly

dx.doi.org/10.1021/ic102493g |*Inorg. Chem.* 2011, 50, 2995–3002

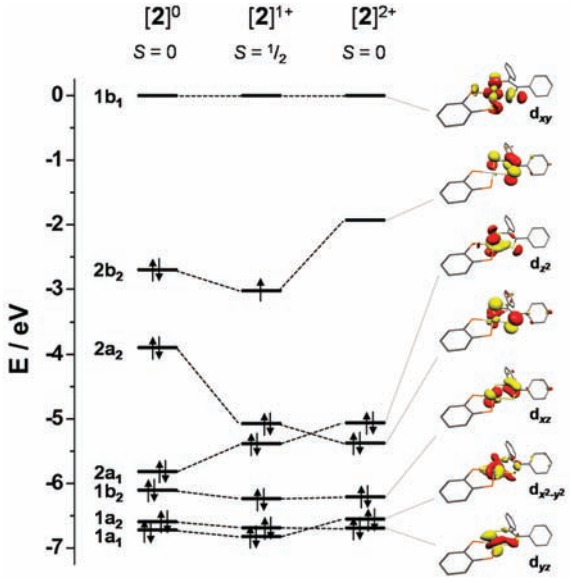

Figure 4. Qualitative MO diagram for the $[\mathbf{2}]^{0/1+/2+}$ electron transfer series from ZORA/B3LYP DFT calculations.

planar (Pd···Pd 9.1 Å), indicating a modest pliability of the molecule that accommodates the demands of crystal packing.

Optimization of the oxidation products, $[\mathbf{1}]^{2+}$ and $[\mathbf{2}]^{1+}$, results in a shortening of the C−S bonds to 1.736 and 1.737 Å, with a concomitant lengthening of the C−C bond to 1.420 Å and 1.421 Å, respectively. The nearly perfect square planarity of the PdP_2S_2 unit is retained, as is the Pd···Pd distance at 9.1 Å in $[\mathbf{1}]^{2+}$, clearly indicating oxidation of each dianionic dithiolene ligand to its monoanionic dithiolene radical form. Further oxidation to generate $[\mathbf{1}]^{4+}$ and $[\mathbf{2}]^{2+}$ leads to the generation of a dithione ligand bound to a Pd(II) metal center rather than metal-centered oxidation, such that this is one of only a handful of systems that assembles all three oxidation levels of the dithiolene ligand.[32]

The qualitative molecular orbital (MO) diagram for **2**, $[\mathbf{2}]^{1+}$, and $[\mathbf{2}]^{2+}$ is available in Figure 4. The highest occupied molecular orbitals (HOMOs) are essentially the C_2S_2 π system ($2b_2$ and $2a_2$ in C_{2v} symmetry) and undergo symmetry-allowed π interactions with the d_{xz} and d_{yz} orbitals, respectively. The miniscule Pd content of 2.5% d_{xz} and 9.8% d_{yz} character in these π^* orbitals, $2b_2$ and $2a_2$, respectively, is a consequence of the high effective nuclear charge of the metal ion that additionally stabilizes the four doubly occupied d orbitals ($d_{x^2-y^2}$, d_{yz}, d_{xz}, d_{z^2}) which account for a Pd(II) d^8 central ion. The lowest unoccupied molecular orbital (LUMO) is a σ^* orbital with 45% d_{xy} character. Oxidation of this neutral species removes one electron from the ligand-based $2b_2$ MO. The Pd content remains unchanged and as such the EPR spectrum of $[\mathbf{2}]^{1+}$ exhibits almost negligible g anisotropy (vide infra).

The electronic structure of **1** is essentially a combination of two **2** molecules, and $[\mathbf{1}]^{2+}$ is generated by simultaneous removal of one electron from each dithiolene ligand. Its electronic structure was calculated using a spin-unrestricted broken symmetry BS(1,1) $M_S = 0$ model, as well as a closed-shell spin-restricted $S = 0$ and spin-unrestricted $S = 1$ states. The closed-shell $S = 0$ solution was found to be a 16.3 kcal mol^{-1} less stable than the BS(1,1) $S = 0$ solution, in contrast to the paltry 0.02 kcal mol^{-1} instability of the $S = 1$ state where the distance between the

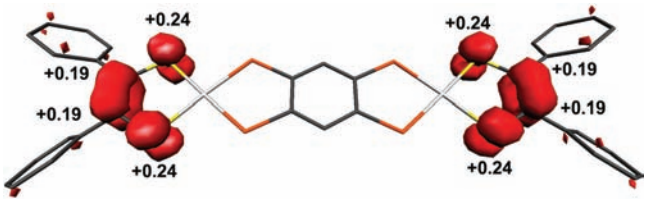

Figure 5. Mulliken spin density plot for the spin-triplet state of $[\mathbf{1}]^{2+}$.

dithiolene ligands ensured a nearly degenerate singlet−triplet ground state for this diradical. The exchange coupling constant was estimated from the high-spin ($S = 1$) and BS energies with the corresponding spin-expectation values $\langle \mathbf{S}^2 \rangle$ according to the Yamaguchi approach, $J' = (E_{HS} - E_{BS})/(\langle \mathbf{S}^2 \rangle_{HS} - \langle \mathbf{S}^2 \rangle_{BS})$,[33] giving $J' = -6.3$ cm^{-1}. This value has been validated by EPR spectroscopy (vide infra). The Mulliken spin population analysis shows one unpaired electron localized on each dithiolene ligand with only 2% spin density on the Pd ions (Figure 5). Further oxidation to $[\mathbf{1}]^{4+}$ and $[\mathbf{2}]^{2+}$ sees the $2b_2$ orbital emptied in accordance with the generation of a dithione ligand (Figure 4).

EPR Spectroscopy. An oxidative coulometric titration of **1** with concurrent monitoring by X-band EPR spectroscopy reveals the initial formation of a paramagnetic species with low g anisotropy typical of an organic radical (Supporting Information, Figure S1). The intensity of the signal continually increases during the two-electron oxidation of **1**, and the new spectral profile includes a shoulder at low field and an apparent splitting and broadening of the lowest g value. The initial spectrum is attributed to the monospin species $[\mathbf{1}]^{1+}$ ($S = {}^1/_2$) that is generated by comproportionation of $[\mathbf{1}]^{2+}$ and **1** (Supporting Information, Figure S3); based on electrochemical data after one electron has been removed, $K_c = 9.6$.[34] The spectrum closely resembles that for $[\mathbf{2}]^{1+}$ (Supporting Information, Figure S5). The final spectrum is attributed to the $S = 1$ state of $[\mathbf{1}]^{2+}$ that is, due to the small singlet−triplet gap, populated at very low temperatures. Unfortunately, efforts to determine this energy gap (represented by the exchange coupling parameter, J') by EPR intensity and Boltzmann depopulations measurements (5 K < T < 50 K) were rendered ineffective by intrinsic line broadening and saturation effects even at low microwave power. However, the magnitude of J' with respect to the Zeeman interaction ($h\nu$ = 0.3 cm^{-1} at X-band) can be appraised by room temperature measurements.

The fluid solution X-band EPR spectrum of $[\mathbf{1}]^{2+}$ shows an isotropic line with faintly visible shoulders from ^{31}P ($I = {}^1/_2$, 100% abundance) superhyperfine coupling (Figure 6 b). Unfortunately, these faint features are not improved at lower frequency (Supporting Information, Figure S4). Nonetheless, both were simulated with $g = 2.008$ and $A_P = 1.35 \times 10^{-4}$ cm^{-1} on the basis of $S = 1$ and four P nuclei.[35] Recourse to $[\mathbf{2}]^{1+}$ ($S = {}^1/_2$) was indispensable in validating these simulation parameters. The fluid solution X-band spectrum of $[\mathbf{2}]^{1+}$ was simulated using $g = 2.008$ and $A_P = 2.70 \times 10^{-4}$ cm^{-1} for $S = {}^1/_2$ and two P nuclei (Figure 6 a);[35] this simulation closely matches an EPR study of near identical compounds.[31] The ^{31}P hyperfine coupling constant is exactly twice that in $[\mathbf{1}]^{2+}$ indicating $|J'| > h\nu$, though still small enough to ensure the triplet state populated at the measurement temperatures (down to 7 K).[7] Therefore, the computed value of $J' = -6.3$ cm^{-1} is in accordance with these fluid solution measurements; however, it should be noted that the sign cannot be ascertained. This result is at odds with the

dx.doi.org/10.1021/ic102493g |Inorg. Chem. 2011, 50, 2995–3002

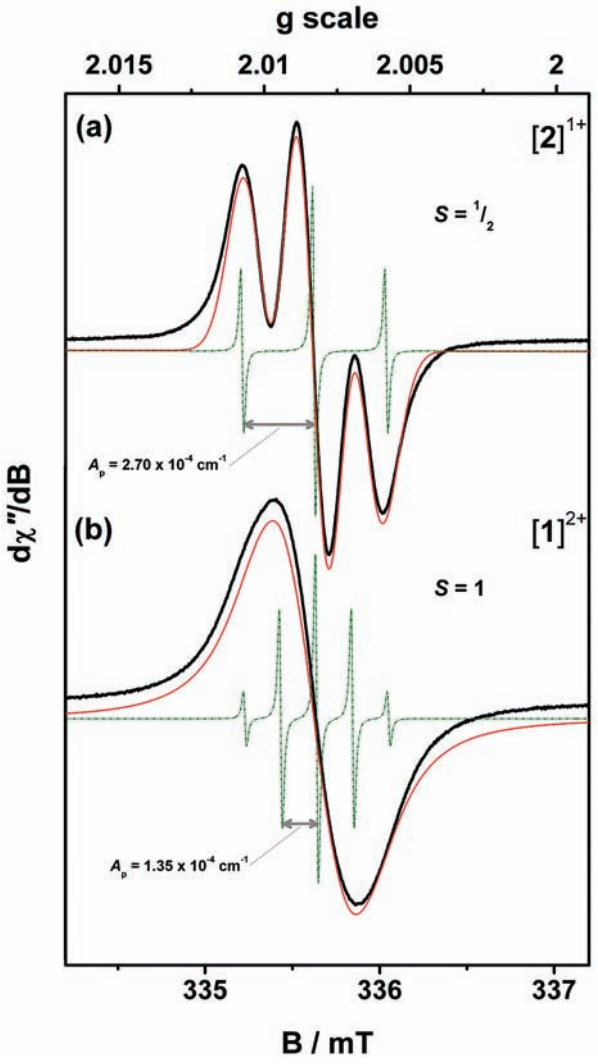

Figure 6. X-band EPR spectra of (a) $[\mathbf{2}]^{1+}$ (conditions: frequency 9.4311 GHz; power 0.63 mW; modulation 0.05 mT), and (b) $[\mathbf{1}]^{2+}$ in CH_2Cl_2 at 295 K (conditions: frequency 9.4331 GHz; power 2.002 mW; modulation 0.05 mT) recorded in CH_2Cl_2 solution at 295 K. The experimental spectra are depicted with a solid line; the red lines represent the simulations, and the green dashed traces depict the simulation with artificially narrow linewidths to contrast the magnitude of ^{31}P superhyperfine coupling in $[\mathbf{2}]^{1+}$ ($S = {}^1/_2$) and $[\mathbf{1}]^{2+}$ ($S = 1$).

conclusion drawn by Wang and Fox.[2] If the spins were indeed localized in their Ni(I)−Ni(I) dimer, then the fluid solution EPR spectrum should have half the ^{31}P hyperfine coupling constant of the monomeric Ni(I) species. It is more likely there exists a very strong antiferromagnetic coupling between the Ni(I) d^9 centers through the Ni−P σ bonds that greatly stabilizes a singlet ground state, such that we postulate decomposition of the dimeric dication to a monomeric species as the most plausible explanation for the observed EPR signal.

The full interaction Hamiltonian for a pair of weakly interacting spins is defined as $\hat{H} = \hat{H}_1 + \hat{H}_2 + \hat{H}_{int}$, where $\hat{H}_1$ and $\hat{H}_2$ are Hamiltonians for the independent spins 1 and 2 in this case described solely by the Zeeman interaction, $\hat{H}_j = \sum \mu_B \mathbf{S}_j \cdot \mathbf{g}_j \cdot \mathbf{B}$, since there is no experimentally observable hyperfine interaction in the frozen solution spectrum. The $\hat{H}_{int}$ term incorporates an isotropic exchange interaction (J') and an anisotropic dipolar

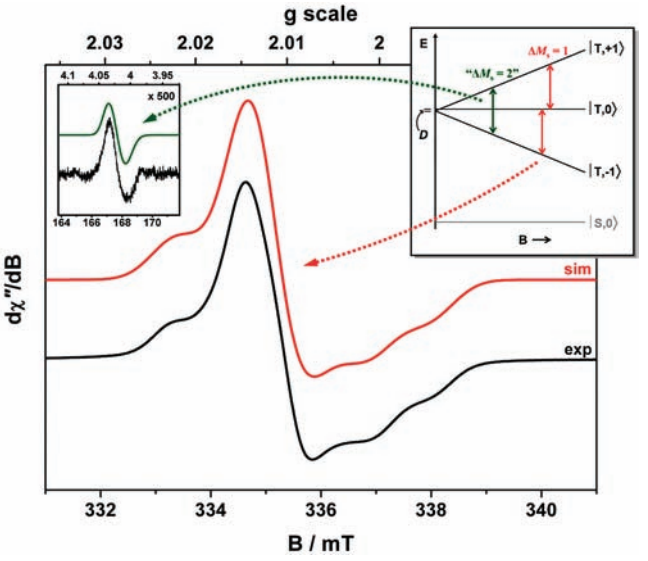

Figure 7. X-band EPR spectrum $[\mathbf{1}]^{2+}$ in CH_2Cl_2 at 30 K. The simulation is shown in red with the experimental spectrum in black (conditions: frequency 9.4352 GHz; power 0.63 mW; modulation 0.5 mT). Inset shows half-field signal at $g = 4.015$ recorded at 7 K (conditions: frequency 9.4363 GHz; power 63 mW; modulation 0.5 mT) and its simulation in green. The spectra have been simulated using $D = -15 \times 10^{-4}$ cm^{-1} and $E/D = 0.008$. The inset right describes the energy level diagram for the spin-triplet of $[\mathbf{1}]^{2+}$, where the allowed $\Delta M_S = 1$ transitions are shown in red and the forbidden half-field "$\Delta M_S = 2$" transition is the green line.

interaction ($\mathbf{J_d}$ is the traceless anisotropic coupling matrix) such that the full spin-Hamiltonian is as defined in eq 1 ($\mathbf{1}$ is the unity matrix).

$$\hat{H}_{pair} = \mathbf{S}_1 \cdot (\mathbf{J_d} - J' \cdot \mathbf{1}) \cdot \mathbf{S}_2 + \sum \mu_B \mathbf{S}_j \cdot \mathbf{g}_j \cdot \mathbf{B} \qquad (1)$$

The frozen solution X-band EPR spectrum of $[\mathbf{1}]^{2+}$ recorded at 30 K was successfully simulated incorporating weak dipolar coupling into an *effective* spin Hamiltonian for a spin-triplet state (eq 2) where D and E/D parameterize the zero-field splitting of the triplet that arises from the anisotropic dipolar part $\mathbf{J_d}$ of the $\mathbf{J}$ interaction matrix used in eq 1.

$$\hat{H} = D[\hat{S}_z^2 - 1/3S(S+1) + E/D(\hat{S}_x^2 + \hat{S}_y^2)] + \mu_B \cdot \mathbf{B} \cdot g \cdot \mathbf{S} \qquad (2)$$

In this approach, singlet−triplet transitions are completely neglected, which is justified by the relatively large J' value. An excellent fit was afforded with minute anisotropy, $g = (2.005, 2.017, 2.004)$ and an amazingly small zero-field splitting, $D = -15 \times 10^{-4}$ cm^{-1} with negligible rhombicity, $E/D = 0.008$ (Figure 7). Furthermore, a very weak forbidden "$\Delta M_S = 2$" transition between pure $|T,+1\rangle$ and $|T,-1\rangle$ triplet levels (Figure 7) at $g = 4.015$ is exposed at 7 K since its intensity is proportional to the magnitude of D (inset, Figure 7).

Since D owes its origin to the dipole interaction between the two dithiolene radicals, its value is a measure of the "mean" separation (r) of the two spin density distributions given by $D = -3/2g^2\mu_B{}^2r^{-3}$ for $E/D = 0$ (where $\mu_B{}^2 = 0.433$ for D in cm^{-1} and r in Å).[8] The value for D of -15×10^{-4} cm^{-1} for $g_x = 2.0052$ obtained by simulation yields a corresponding distance of 12.0 Å between the two radicals, where the x-axis bisects the dithiolene and tpbz ligands.[36] This approximation fits closely to the

dx.doi.org/10.1021/ic102493g |Inorg. Chem. 2011, 50, 2995–3002

interspin distance derived from geometry optimization of $[\mathbf{1}]^{2+}$ because of the negligible rhombicity of the zero-field splitting. Moreover, using the ratio of the intensity of the "$\Delta M_S = 2$" transition to the $\Delta M_S = 1$ transitions, and the correlation curve generated by Eaton and Eaton,[6] we derive an interspin distance of 12.12 Å. This methodology is again exclusive of rhombicity but does reveal the effect of intermolecular interactions that would increase the ratio, since the "$\Delta M_S = 2$" transition intensity for intermolecular interactions is dependent on the square of the concentration, whereas it is linear for the $\Delta M_S = 1$ transitions. It can be seen these are not prominent in this system, because of a combination of the complex charge and the steric bulk provided by the multitude of phenyl substituents.

A more sophisticated approach lies with the construction of a multipoint dipole model that accommodates the distribution of spin density across the C_2S_2 π system (Supporting Information, Figure S7). Using the Mulliken population analysis for ligand spin in predominantly the p_z orbitals of the carbon and sulfur atoms, dipole−dipole simulations were based on the geometry optimized structure for $[\mathbf{1}]^{2+}$, where the distance between the spin origins (the centroid of the dithiolene S atoms) is 12.434 Å. Quite astonishingly, zero-field splitting parameters $D = -15.31 \times 10^{-4}$ cm^{-1} and $E/D = 0.0077$ were computed. It should be noted that E/D is unaffected by structural distortions such as introducing a chairlike conformation to the Pd-tpbz-Pd unit, increasing tetrahedralization of the Pd centers, and bowing along the length of the molecule. The latter distortion shortens the interspin distance, leading to an increase in D and a widening of the spectrum around $g = 2$ (Supporting Information, Figure S8).

CONCLUSIONS

We have shown that the rather facile two-electron oxidation of **1** generates two coordinated dithiolene radicals. The stabilization of the Pd d manifold with respect to the dithiolene donor orbitals and the absence of suitable π orbitals on the bridging tetraphosphine, generates a very weak spin−spin interaction. This interaction is manifested in the EPR spectrum with an extremely rare occurrence in which the g anisotropy (∼2.0 mT) is equivalent to the zero-field splitting (∼1.6 mT) of the spin-triplet state, giving rise to a faint half-field signal that was only visible at low temperatures with very high power.

Through understanding this simple system, **1** can be used as an elementary unit in the construction of more elaborate multimetallic compounds with Pd(II) ions interspaced by insulating tetraphosphine bridges and redox-active benzenetetrathiolate linkages.[5] Furthermore, the system can be tailored by variation of the ligand substituents such that deliberate shifts of the redox potentials can be effected. Recent spectroscopic and theoretical studies of transition metal bis- and tris(dithiolene) complexes have detailed the electronic and molecular structure permutations accessible by judicious selection of the metal ion, with the rigid square planar geometry imposed by Ni, Pd, Pt, and Au,[37] octahedral centers with Fe and Co,[38,39] and a preference for trigonal prismatic arrangements by V and Re.[40] These adaptations can be simply introduced in a concerted stepwise synthetic strategy,[5,41] with a multitude of different metal ions leading to molecular, oligomeric, or polymeric species. The enhanced and tunable properties that such materials should display suggest their potential use in a variety of applications ranging from chemical sensors for binding of small molecules[39,42] to spin qubits for quantum computing.

ASSOCIATED CONTENT

Supporting Information. X-ray crystallographic files in CIF format for **1** and **2**. X-band EPR spectra of $[\mathbf{1}]^{1+}$ and $[\mathbf{2}]^{1+}$, S-band fluid solution EPR spectrum of $[\mathbf{1}]^{2+}$, and details of the multipoint dipole model dimensions. Tables of geometric and electronic structures details (qualitative MO schemes and Mulliken spin density plots) of all calculated structures. This material is available free of charge via the Internet at http://pubs.acs.org.

AUTHOR INFORMATION

Corresponding Author

*E-mail: sproules@mpi-muelheim.mpg.de (S.S.), donahue@tulane.edu (J.P.D.).

ACKNOWLEDGMENT

This work is supported by NSF grant CHE-0845289 (J.P.D.) and by the Fonds der Chemischen Industrie. S.S. thanks the Max-Planck-Society for a postdoctoral fellowship.

REFERENCES

(1) Lehn, J.-M. *Supramolecular Chemistry*; VCH: Weinheim, Germany, 1995.
(2) Wang, P.-W.; Fox, M. A. *Inorg. Chem.* **1994**, *33*, 2938.
(3) (a) Fox, M. A.; Chandler, D. A. *Adv. Mater.* **1991**, *3*, 381. (b) Wang, P.-W.; Fox, M. A. *Inorg. Chem.* **1995**, *34*, 36.
(4) (a) Affronte, M.; Casson, I.; Evangelisti, M.; Candini, A.; Carretta, S.; Muryn, C. A.; Teat, S. J.; Timco, G. A.; Wernsdorfer, W.; Winpenny, R. E. P. *Angew. Chem., Int. Ed.* **2005**, *44*, 6496. (b) Amico, L.; Fazio, R.; Osterloh, A.; Vedral, V. *Rev. Mod. Phys.* **2008**, *80*, 517. (c) Timco, G. A.; Carretta, S.; Troiani, F.; Tuna, F.; Pritchard, R. J.; Muryn, C. A.; McInnes, E. J. L.; Ghirri, A.; Candini, A.; Santini, P.; Amoretti, G.; Affronte, M.; Winpenny, R. E. P. *Nat. Nanotechnol.* **2009**, *4*, 173. (d) Winpenny, R. E. P. *Angew. Chem., Int. Ed.* **2008**, *47*, 7992.
(5) Arumugam, K.; Shaw, M. C.; Chandrasekaran, P.; Villagrán, D.; Gray, T. G.; Mague, J. T.; Donahue, J. P. *Inorg. Chem.* **2009**, *48*, 10591.
(6) Eaton, S. S.; Eaton, G. R. *J. Am. Chem. Soc.* **1982**, *104*, 5002.
(7) Eaton, G. R.; Eaton, S. S. *Acc. Chem. Res.* **1988**, *21*, 107.
(8) Eaton, S. S.; More, K. M.; Sawant, B. M.; Eaton, G. R. *J. Am. Chem. Soc.* **1983**, *105*, 6560.
(9) (a) McFarlane, H. C. E.; McFarlane, W. *Polyhedron* **1999**, *18*, 2117. (b) McFarlane, H. C. E.; McFarlane, W. *Polyhedron* **1988**, *7*, 1875.
(10) McFarlane, H. C. E.; McFarlane, W. *Polyhedron* **1983**, *2*, 303.
(11) Menozzi, E.; Busi, M.; Ramingo, R.; Campagnolo, M.; Geremia, S.; Dalcanale, E. *Chem.—Eur. J.* **2005**, *11*, 3136.
(12) Chandrasekaran, P.; Arumugam, K.; Jayarathne, U.; Pérez, L. M.; Mague, J. T.; Donahue, J. P. *Inorg. Chem.* **2009**, *48*, 2103.
(13) Armarego, W. L. F.; Perrin, D. D. *Purification of Laboratory Chemicals*, 4th ed.; Butterworth-Heinemann: Oxford, Great Britain, 2000.
(14) *APEX2*, Version 2009 1-0; Bruker-AXS: Madison, WI, 2009.
(15) Sheldrick, G. M. *CELL_NOW*, Version 2008/2; Universität Göttingen: Göttingen, Germany, 2008.
(16) *SAINT*, Version 7.60A; Bruker AXS: Madison, WI, 2008.
(17) (a) Sheldrick, G. M. *SADABS*, Version 2008/2; Universität Göttingen: Göttingen, Germany, 2008. (b) Sheldrick, G. M. *TWINABS*, Version 2008/3; Universität Göttingen: Göttingen, Germany, 2008.
(18) (a) *SHELXTL*, Version 2008/4; Bruker-AXS: Madison, WI, 2008. (b) Sheldrick, G. M. *SHELXS97 and SHELXL97*; Universität Göttingen: Göttingen, Germany, 2008.
(19) Spek, A. L. *PLATON, A Multipurpose Crystallographic Tool*; Utrecht University: Utrecht, The Netherlands, 2009.
(20) Hanson, G. R.; Gates, K. E.; Noble, C. J.; Griffin, M.; Mitchell, A.; Benson, S. *J. Inorg. Biochem.* **2004**, *98*, 903.

(21) Neese, F. *Orca, an Ab Initio, Density Functional and Semiempirical Electronic Structure Program Package*, version 2.7, revision 1523; Universität Bonn: Bonn, Germany, 2010.
(22) (a) Becke, A. D. *J. Chem. Phys.* **1988**, *84*, 4524. (b) Perdew, J. P. *Phys. Rev. B* **1986**, *33*, 8822.
(23) Weigend, F.; Ahlrichs, R. *Phys. Chem. Chem. Phys.* **2005**, *7*, 3290.
(24) (a) van Lenthe, E.; Faas, S.; Snijders, J. G. *Chem. Phys. Lett.* **2000**, *328*, 107. (b) van Lenthe, E.; Snijders, J. G.; Baerends, E. J. *J. Chem. Phys.* **1996**, *105*, 6505.
(25) van Lenthe, E.; van der Avoird, A.; Wormer, P. E. S. *J. Chem. Phys.* **1998**, *98*, 5648.
(26) Klamt, A.; Schuuramann, G. *J. Chem. Soc., Perkin Trans.* **1993**, *2*, 793.
(27) (a) Pulay, P. *Chem. Phys. Lett.* **1980**, *73*, 393. (b) Pulay, P. *J. Comput. Chem.* **1992**, *3*, 556.
(28) (a) Becke, A. D. *J. Chem. Phys.* **1993**, *98*, 5648. (b) Lee, C. T.; Yang, W. T.; Parr, R. G. *Phys. Rev. B* **1988**, *37*, 785.
(29) (a) Noodleman, L. *J. Chem. Phys.* **1981**, *74*, 5737. (b) Noodleman, L.; Case, D. A.; Aizman, A. *J. Am. Chem. Soc.* **1988**, *110*, 1001. (c) Noodleman, L.; Davidson, E. R. *Chem. Phys.* **1986**, *109*, 131. (d) Noodleman, L.; Norman, J. G.; Osborne, J. H.; Aizman, A.; Case, D. A. *J. Am. Chem. Soc.* **1985**, *107*, 3418. (e) Noodleman, L.; Peng, C. Y.; Case, D. A.; Monesca, J. M. *Coord. Chem. Rev.* **1995**, *144*, 199.
(30) *Molekel, Advanced Interactive 3D-Graphics for Molecular Sciences*; Swiss National Supercomputing Center: Lugano, Switzerland; http://www.cscs.ch/molekel.
(31) Bowmaker, G. A.; Boyd, P. D. W.; Campbell, G. K. *Inorg. Chem.* **1983**, *22*, 1208.
(32) (a) Bigoli, F.; Cassoux, P.; Deplano, P.; Mercuri, M. L.; Pellinghelli, M. A.; Pintus, G.; Serpe, A.; Trogu, E. F. *J. Chem. Soc., Dalton Trans.* **2000**, 4639. (b) Bigoli, F.; Chen, C.-T.; Wu, W.-C.; Deplano, P.; Mercuri, M. L.; Pellinghelli, M. A.; Pilia, L.; Pintus, G.; Serpe, A.; Trogu, E. F. *Chem. Commun.* **2001**, 2246. (c) Geary, E. A. M.; Yellowlees, L. J.; Parsons, S.; Pilia, L.; Serpe, A.; Mercuri, M. L.; Deplano, P.; Clark, S. J.; Robertson, N. *Dalton Trans.* **2007**, 5453. (d) Noh, D.-Y.; Seo, E.-M.; Lee, H.-J.; Jang, H.-Y.; Choi, M.-G.; Kim, Y. H.; Hong, J. *Polyhedron* **2001**, *20*, 1939.
(33) Soda, T.; Kitagawa, Y.; Onishi, T.; Takano, Y.; Shigeta, Y.; Nagao, H.; Yoshioka, Y.; Yamaguchi, K. *Chem. Phys. Lett.* **2000**, *319*, 223.
(34) The equilibrium constant for $[\mathbf{1}]^{0} + [\mathbf{1}]^{2+} \rightarrow 2[\mathbf{1}]^{1+}$ was evaluated by $K_c = e^{(\Delta E \bullet nF/RT)}$ after 50% of the charge had been removed such that the concentration of $[\mathbf{1}]^{0}$ and $[\mathbf{1}]^{2+}$ are equivalent. $\Delta E_{1/2}$ (the difference in potential for the $[\mathbf{1}] \rightarrow [\mathbf{1}]^{1+}$ and the $[\mathbf{1}]^{1+} \rightarrow [\mathbf{1}]^{2+}$ oxidations) is assessed as 58 mV from the differential pulse voltammogram of $[\mathbf{1}]$ using the width-at-half-height method described by Richardson, D. E.; Taube, H. *Inorg. Chem.* **1981**, *20*, 1278.
(35) Fluid solution spectra were simulated using $\hat{H} = \mathbf{g} \cdot \mu_B \cdot \mathbf{B} \cdot \mathbf{S} + \sum a_j \cdot \mathbf{S} \cdot I$, where $S = 1$ for $[\mathbf{1}]^{2+}$ and $S = {}^1/_2$ for $[\mathbf{2}]^{1+}$.
(36) Kirmse, R.; Stach, J.; Dietzsch, W.; Steimecke, G.; Hoyer, E. *Inorg. Chem.* **1980**, *19*, 2679.
(37) (a) Ray, K.; Weyhermüller, T.; Neese, F.; Wieghardt, K. *Inorg. Chem.* **2005**, *44*, 5345. (b) Szilagyi, R. K.; Lim, B. S.; Glaser, T.; Holm, R. H.; Hedman, B.; Hodgson, K. O.; Solomon, E. I. *J. Am. Chem. Soc.* **2003**, *125*, 9158.
(38) (a) Ray, K.; Begum, A.; Weyhermüller, T.; Piligkos, S.; van Slageren, J.; Neese, F.; Wieghardt, K. *J. Am. Chem. Soc.* **2005**, *127*, 4403. (b) Ray, K.; Bill, E.; Weyhermüller, T.; Wieghardt, K. *J. Am. Chem. Soc.* **2005**, *127*, 5641.
(39) Sproules, S.; Wieghardt, K. *Coord. Chem. Rev.* **2010**, *254*, 1358.
(40) (a) Sproules, S.; Benedito, F. L.; Bill, E.; Weyhermüller, T.; DeBeer George, S.; Wieghardt, K. *Inorg. Chem.* **2009**, *48*, 10926. (b) Sproules, S.; Weyhermüller, T.; DeBeer, S.; Wieghardt, K. *Inorg. Chem.* **2010**, *49*, 5241.
(41) Arumugam, K.; Yu, R.; Villagrán, D.; Gray, T. G.; Mague, J. T.; Donahue, J. P. *Inorg. Chem.* **2008**, *47*, 5570.
(42) Yu, R.; Arumugam, K.; Manepalli, A.; Tran, Y.; Schmehl, R.; Jacobsen, H.; Donahue, J. P. *Inorg. Chem.* **2007**, *46*, 5131.